# Supramolecular Functionalization and Concomitant Enhancement in Properties of $Au_{25}$ Clusters

**Ammu Mathew,[†] Ganapati Natarajan,[†] Lauri Lehtovaara,[‡] Hannu Häkkinen,[‡] Ravva Mahesh Kumar,[§] Venkatesan Subramanian,[§] Abdul Jaleel,[⊥] and Thalappil Pradeep[†,*]**

[†]DST Unit of Nanoscience (DST UNS) and Thematic Unit of Excellence, Department of Chemistry, Indian Institute of Technology Madras, Chennai 600036, India, [‡]Departments of Chemistry and Physics, Nanoscience Center, University of Jyväskylä, 40014 Jyväskylä, Finland, [§]Chemical Laboratory, CSIR-Central Leather Research Institute, Adyar, Chennai 600020, India, and [⊥]Proteomics Core Facility, Rajiv Gandhi Centre for Biotechnology, Thiruvananthapuram 695014, India

**ABSTRACT** We present a versatile approach for tuning the surface functionality of an atomically precise 25 atom gold cluster using specific host–guest interactions between $\beta$-cyclodextrin (CD) and the ligand anchored on the cluster. The supramolecular interaction between the $Au_{25}$ cluster protected by 4-(*t*-butyl)benzyl mercaptan, labeled $Au_{25}SBB_{18}$, and CD yielding $Au_{25}SBB_{18}\cap CD_n$ ($n$ = 1, 2, 3, and 4) has been probed experimentally using various spectroscopic techniques and was further analyzed by density functional theory calculations and molecular modeling. The viability of our method in modifying the properties of differently functionalized $Au_{25}$ clusters is demonstrated. Besides modifying their optoelectronic properties, the CD moieties present on the cluster surface provide enhanced stability and optical responses which are crucial in view of the potential applications of these systems. Here, the CD molecules act as an umbrella which protects the fragile cluster core from the direct interaction with many destabilizing agents such as metal ions, ligands, and so on. Apart from the inherent biocompatibility of the CD-protected Au clusters, additional capabilities acquired by the supramolecular functionalization make such modified clusters preferred materials for applications, including those in biology.

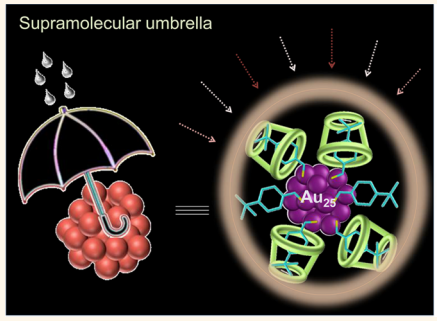


**KEYWORDS:** supramolecular chemistry · quantum clusters · $Au_{25}$ · cyclodextrin · inclusion complex

Distinct properties of nanomaterials arise from diverse attributes, the most important being size, shape, chemical functionalization, and interparticle organization.[1−3] Interfacing individual nanoparticles with functional supramolecular systems is a fascinating prospect which provides them with new capabilities. In this paper, we introduce a method for such surface modifications in atomically precise gold clusters, which are emerging materials due to their unique optical and catalytic properties.[4−8] They are called by various names such as quantum clusters (QCs), nanomolecules, molecular clusters, superatoms, *etc.* Unique molecule-like absorption (especially that of $Au_{25}SR_{18}$ (SR denotes the surface thiolate ligand)) and photoluminescence properties of QCs are the result of confinement of electronic wavefunctions[4,5,9−11] which can be manipulated by the modification of the ligand environment.[12−15] The physicochemical interactions occurring at the surface of QCs may change the efficiency of radiative recombination, which may ultimately result in the enhancement or quenching of their optical properties. QCs, as tunable nanoscale light sources, have found numerous applications in biology, bioanalytics, and optoelectronics.[16−19] Many of these applications require engineering of their surfaces with functional ligands. Different approaches have been developed to achieve this, such as ligand exchange[7] and subsequent isolation of clusters with precise composition,[20] click chemistry, and so on.[21−25] As a complementary and even more versatile concept, especially for solution-state applications, we introduce the possibility of supramolecular chemistry with QCs, which enables their precise surface functionalization with molecules that can take part in additional events. These surface modifications are important to enable the use of diverse properties of such molecular nanosystems.[26]

Being the most popular supramolecular host molecule, $\beta$-cyclodextrin ($\beta$-CD), cyclic

* Address correspondence to pradeep@iitm.ac.in.

Received for review May 17, 2013 and accepted December 6, 2013.

**Published online December 06, 2013**
**10.1021/nn406219x**

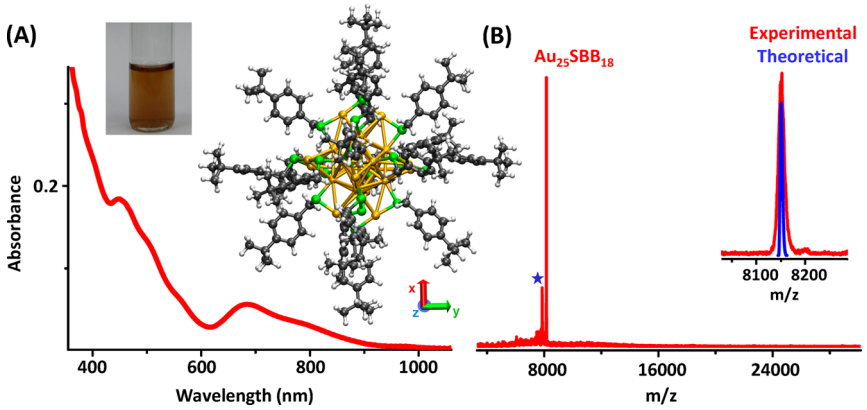


**Figure 1. UV−vis absorption spectra (A) and MALDI (L) mass spectra in the positive ion mode (B) of $Au_{25}SBB_{18}$. Inset shows a photograph of the cluster (diluted) in THF. Inset of (A) also shows a visualization of the DFT-optimized structure of $Au_{25}SBB_{18}$. Gold atoms are shown in gold, sulfur atoms in green, carbon atoms in dark gray, and hydrogen atoms in white. The bridging sulfurs lie along Cartesian axis directions. Here, $Au_{25}SBB_{18}$ and its Cartesian axes have been oriented so that the environment around the ligands can be seen clearly. In this particular orientation, the $x-y$ plane is in the plane of the paper as shown by the red and green arrows, and the $z$-axis is going into the plane of the paper as indicated by the blue arrow. Inset of (B) compares the theoretically calculated and experimentally observed molecular ion peak of the cluster. A fragment of ionization $(Au_{25}SBB_{16}S_2)^+$ is marked by ∗. The peak at $m/z$ 8151 is due to $Au_{25}SBB_{18}$.**

oligosaccharide comprising seven α-D-glucopyranose units linked by α(1−4) glycosidic bonds, has molecule-accepting cavities which are specific to hydrophobic guest molecules of suitable size and geometry.[26] In addition to other applications, this feature has been exploited for the design and construction of molecular sensors in which the inclusion of the guest molecule triggers a signal which can be detected.[27,28] Binding of β-CD molecules to various guest-functionalized materials has been utilized for various applications in water purification and biology.[29−31] Owing to the high vulnerability of the 4-(*t*-butyl)benzyl group to form stable host/guest inclusion complexes with β-CD molecules, we synthesized a new 25 atom gold QC protected by 4-(*t*-butyl)benzyl mercaptan (BBSH) and explored its precise surface functionalization with β-CD molecules. The partial inclusion complex formed due to the host−guest interactions between β-CD and SBB ligand anchored on the $Au_{25}$ cluster may be represented as X∩Y, where X and Y are substrate and receptor molecules, respectively, as suggested by Lehn[32] and colleagues.[33] Strong inclusion interactions between the inner cavity of β-CD and ligand molecules on the QC have been probed by various spectroscopic techniques and density functional theory (DFT) calculations. Detailed studies on the stability of the functionalized cluster in the presence of metal ions and ligands have also been performed. As the binding of the substrate to its receptor involves a molecular recognition process, presence of a more competitive guest molecule can effectively tune the host−guest reactivity and alter the supramolecular environment around the cluster, suggesting potential applications in sensing. Beyond enhanced stability and sensing properties, creating such precise CD-functionalized clusters can lead to numerous applications in biology and therapeutics since such materials can be envisaged to develop drug delivery vehicles that can be tracked simultaneously.

## RESULTS AND DISCUSSION

There is a strong motivation for making quantum clusters protected with ligands as we wish to use their molecular recognition properties to build supramolecular structures. Here, we synthesized a 25 atom QC of gold with remarkable stability using BBSH as the ligand by following a facile one-pot strategy. BBSH was chosen as the ligand due to its strong tendency to form an inclusion complex with β-CD (binding constant and other data are presented later in the text). The bulkiness of this ligand, while reported to provide higher oxidation resistance to larger Ag clusters ($Ag_{140}$ and $Ag_{\sim 280}$), was also viewed as a challenge for the synthesis of clusters with smaller cores.[34,35] The formation of a well-characterized $Au_{25}$ cluster with BBSH ligand throws light onto the possibility of such smaller core sizes with Ag, too. In view of various reports on the $Au_{25}$ core, protected with other ligands such as GSH and PET,[5,11,36] we present only the relevant characteristics of $Au_{25}SBB_{18}$ in the main text. Most of the other spectroscopic and microscopic data are presented in Supporting Information (SI).

The cluster has well-defined optical and mass spectral features. The optical absorption spectrum (Figure 1A) of the dark brownish solution revealed discrete molecule-like features which are characteristic, and often described, as the fingerprint of $Au_{25}$ QCs.[5,7,37] A key parameter which decides the formation of $Au_{25}SBB_{18}$

is the molar ratio of Au and BBSH, which significantly affects the yield of $Au_{25}$. While the formation of $Au_{25}SBB_{18}$ required a ratio of 1:6 at an optimized condition, lower thiol ratios resulted in larger clusters which were noticeable from the changes in the optical absorption spectra (see Figure S1 in SI).

The molecular composition of the cluster was confirmed by MALDI (L) MS, where L denotes analysis in the linear mode (Figure 1B). An intact molecular ion peak was observed at *m/z* 8151, which also indicated the purity of the prepared cluster. The experimental spectrum and the theoretical prediction matched perfectly as shown in the inset of Figure 1B. Molecular ion peak was observed in both the positive and the negative ion modes (Figure S2). An additional fragment corresponding to the C−S bond cleavage (marked with an asterisk in Figure 1) was observed. Due to the bulky nature of the ligand, a mass loss of *m/z* 294 corresponding to two BB groups ($-CH_2-C_6H_4-C(CH_3)_3$) from the parent cluster was identified apart from peaks due to the loss of $Au_4SBB_4$ from the parent ion (see Figure S2), a common phenomenon observed in such $Au_{25}$ clusters.[11,38] A precise control of the threshold laser intensity was crucial to observe the molecular ion peak without fragmentation (Figure S3). A DFT-optimized model of $[Au_{25}SBB_{18}]^-$ is shown in the inset of Figure 1A. While the core and staple motifs are preserved from the $Au_{25}PET_{18}$ case, there are differences in the directions of the SBB ligands when compared to their PET counterparts, and these are attributed to differences in the rotation angles of ligands about their S−C bonds. We note that, in general, the SBB ligands point away from the core, enabling their inclusion into CD. This scenario may be contrasted with that of $Au_{25}PET_{18}$, where the ligands do not point outward from the core,[37] and hence it would be difficult for a CD to form an inclusion complex with it (see later). ESI MS of the cluster (Figure S4) in the negative mode yielded fragments in the low mass region corresponding to $(AuSBB_2)^-$, $(Au_2SBB_3)^-$, $(Au_3SBB_4)^-$, and $(Au_4SBB_5)^-$ due to fragmentation of staples from the cluster surface. The average size of the cluster was <2 nm as confirmed by TEM (Figure S5), and it did not show any electron-beam-induced aggregation, a common phenomenon observed in other Ag and Au clusters. This may be due to the better stability provided by the bulky ligand shell around the cluster. Elemental analysis of the cluster (Figure S6) showed a Au/S ratio of 1:0.73, in agreement with $Au_{25}SBB_{18}$. With the confirmation that the cluster formed is $Au_{25}SBB_{18}$, we move to the construction of the supramolecular adducts.

The 4-(*t*-butyl)benzyl group of the SBB ligand on $Au_{25}$ is an interesting entity as it acts as a recognition site for stable host/guest inclusion complexes with $\beta$-CD molecules. Pure and modified CDs have been widely documented to form stable host/guest inclusion complexes with hydrophobic molecules of appropriate size so as to be included in its cavity.[39,40] Such complexes are stable, and the products can be isolated. Several inorganic complexes bearing 4-(*t*-butyl)phenyl groups have been reported to form stable host/guest complexes with $\beta$-CD.[41−45] $Au_{25}SBB_{18}\cap CD_n$ ($n$ = 1−4) were made as described in the Experimental Methods section. Initially, the $Au_{25}SBB_{18}$ cluster in THF was mixed with different mole ratios of CD in water and subjected to sonication. Though CD host−guest interactions are known to be most powerful in water, yield of the CD-functionalized cluster analogues (as observed in ESI MS) was poor when the experiment was conducted under conditions of excess water. The tendency of $Au_{25}SBB_{18}$ to aggregate in highly polar medium may prevent the efficient interaction between CD and the guest molecules from forming inclusion complexes in excess water. The CD molecules themselves form tubular assemblies specifically in THF medium,[46] and this formation is facilitated by the presence of small amounts of water.[46,47] This was confirmed from SEM observations (Figure S7). Intermolecular H bonding between the hydroxyl groups on the outer rim of CD molecules, mediated by water, holds them together to form the assembly. Such channel structures of CDs are capable of forming inclusion complexes.[46,47] During the formation of such superstructures, the SBB group present on the cluster may also get entrapped inside the CD cavity. Addition of excess water results in the collapse of CD assemblies releasing the $Au_{25}SBB_{18}\cap CD_n$ adducts.

Cluster-entrapped supramolecular adducts of CD ($Au_{25}SBB_{18}\cap CD_n$, where $n$ = 1−4) can be extracted into the organic layer. Due to the presence of more hydrophobic SBB groups on the cluster surface ($18 - n$, where $n < 4$), the adducts are hydrophobic in nature and allow this preferential extraction into the organic layer. In agreement with this, LDI MS of the aqueous layer showed a broad peak at higher mass range albeit with very low intensity (Figure S8). We noticed that the intensities of MALDI and ESI MS spectra of the CD-incorporated $Au_{25}$ cluster in the crude product (before adding excess water) were weak, whereas a significant enhancement in the adduct intensities was observed in both MALDI and ESI MS after addition of excess water. The purified organic layer, devoid of free CD molecules, was used for subsequent characterization as described in the Experimental Methods section. The hydrophobic interactions between the SBB ligand-protected $Au_{25}$ cluster and $\beta$-CD were studied by a combination of absorption, fluorescence, MALDI MS, ESI MS, and NMR spectroscopies.

MALDI MS of the cleaned organic layer was done with linear (MALDI (L)) and reflectron modes (denoted as MALDI (R)) as well as in TOF TOF mode (MALDI TOF TOF). MALDI (L) MS (Figure S9) measurements of the cluster−CD adduct resulted in a broadened mass spectrum. Factors such as ion kinetic energy distribution of the ejected ions as well as their spatial and temporal distributions are strongly influenced by the

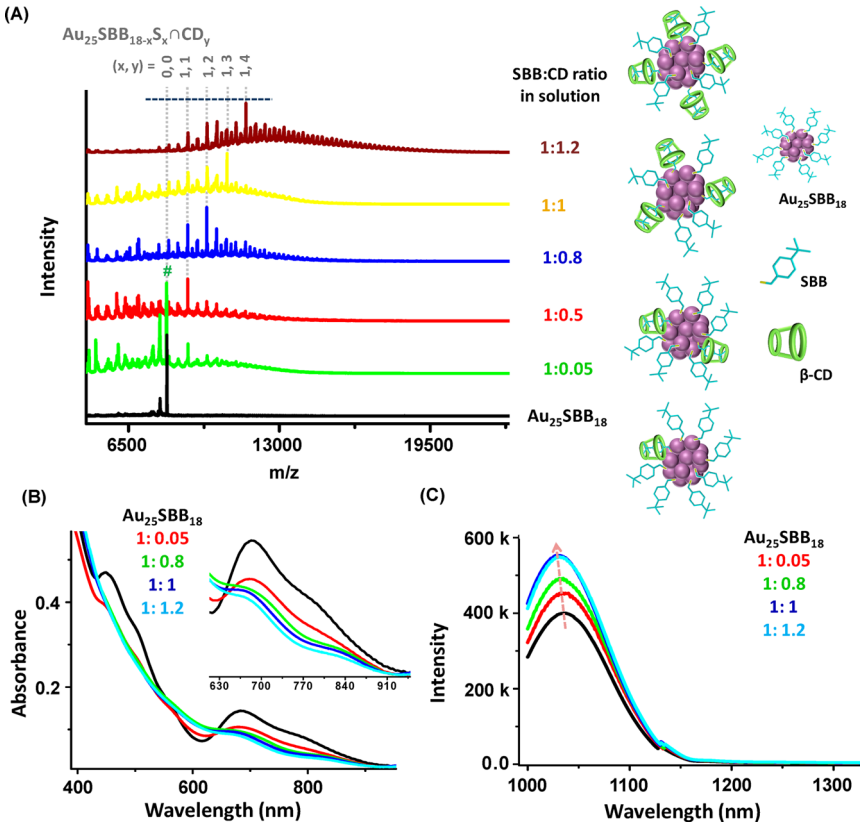


**Figure 2. (A) Effect of MALDI TOF TOF mass spectra of $Au_{25}SBB_{18}$ (black trace) with increasing SBB/CD ratio (green to brown trace) in solution. Schematic representations of the cluster with different amounts of CD inclusions are also shown. At 1:0.05, some parent $Au_{25}SBB_{18}$ is also seen, shown with #. UV−vis absorption spectra (B) and luminescence spectra ($\lambda_{ex}$ 992 nm) (C) of the $Au_{25}SBB_{18}$ cluster with increasing amounts of CD inclusion.**

molecular weight, nature of ions, and the matrix,[48,49] which are important in the present case in determining the spectral width. Though the peaks were broad, the peak maximum of samples made with increasing CD concentration in solution shifted toward higher mass numbers, suggesting the complexation of $\beta$-CD on the cluster surface. The difference in energy distribution of the ions arising from the desorption ionization event, the possibility of large internal energy distributions of the ejected ions as well as metastable fragmentation due to the presence of flexible supramolecular interactions may be the reason for the significant spread for the ions.[50−53] This spread is evidenced from the fact that the broad distributions in MALDI (L) MS transform to narrow lines over a broad background in the TOF TOF mode with the MALDI (R) MS giving an intermediate distribution. Figure S9 compares the MALDI (L) and MALDI (R) mass spectra.

To confirm this, MALDI TOF TOF mass spectra of mixtures of various SBB/CD ratios were collected wherein better peak resolutions were obtained, as shown in Figure 2A, indicating that improved resolution requires TOF TOF measurements and longer path lengths. The mole ratio of SBB ligand to $\beta$-CD in solution for each case is indicated on the figure. Schematic representations of the cluster with various amounts of CD inclusions are also shown in Figure 2. Peak corresponding to the parent $Au_{25}SBB_{18}$ is marked with #. Spectra corresponding to intermediate SBB/CD ratios are shown in Figure S10. Well-defined peaks corresponding to $Au_{25}SBB_{18}\cap CD_n$ (where $n$ = 1−4) were observed under different conditions. The trend observed in CD adduct intensities with an increase in SBB/CD is the same as seen in MALDI MS (Figure S9), confirming that the energy spread of the ions in MALDI MS was the reason for the poor resolution.

As in the case of ligand exchange reactions of clusters,[20,54−56] at each ratio of reactants, one can observe multiple peaks due to the existence of various species in solution. However, formation of certain cluster−adduct combinations is indeed higher than the others depending on the incoming $\beta$-CD concentration. While a statistical distribution of species always exists in solution and precise control of the formation of exclusively one adduct is difficult, it is indeed possible to create one particular adduct with a higher proportion than the rest by careful control of the precursor ratios.[57] The relative intensities of individual peaks shown in Figure 2A for each ratio suggest such an effect.

It may be noted that optimum laser fluence (lowest fluence needed to observe ion signals) was used for all

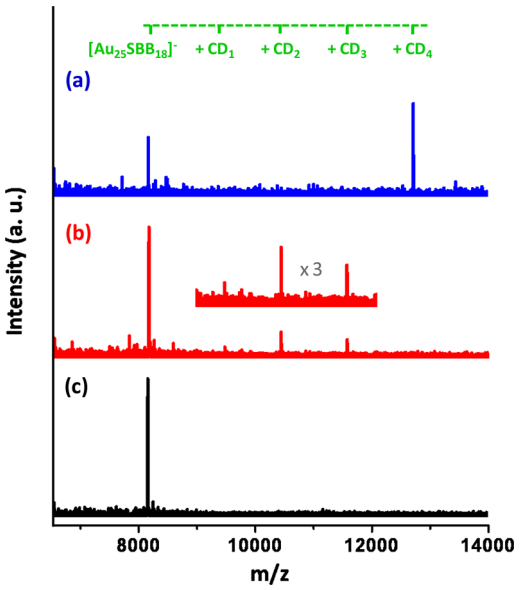


**Figure 3. ESI mass spectra in the negative mode for $[Au_{25}SBB_{18}]^-$ and its CD-functionalized analogues collected using a Q TOF (Synapt G2 HDMS, Waters) mass spectrometer (details are in the Instrumentation section). SBB/CD ratios used for the synthesis were 1:1.2, 1:1, and 1:0 for traces a to c, respectively. Part of trace b is expanded to show the features clearly.**

the measurements. The dependence of laser fluence on both the MALDI and MALDI TOF TOF mass spectra for $Au_{25}SBB_{18}\cap CD_4$ is shown in Figure S11. It is also important to mention that the MALDI event can cause fragmentation of the adducts and part of the distribution of the lower mass ions may also be due to this. Ion/molecule reactions in the plasma can lead to gas-phase products at higher masses, not originally present in solution. All of these aspects are inherent complications in the spectrum, and therefore, it is important to study the product distribution using other methods.

We conducted extensive ESI MS measurements to understand the existence of various species in solution. Spectrum in the negative mode confirmed the mass assignment mentioned earlier. Figure 3 shows distinct peaks corresponding to various $Au_{25}SBB_{18}\cap CD_n$ (where $n = 2-4$) clusters. Unlike MALDI, matrix interactions and laser-induced fragmentation of the products can be avoided in this case. Although at lower ratios the parent $Au_{25}$ peak was dominant compared to the adducts (for $n = 2$ and 3) and multiple species existed in solution, at a SBB/CD ratio of 1:1.2, greater abundance for $Au_{25}SBB_{18}\cap CD_4$ species was seen. A possible reason could be the geometric stability of the $Au_{25}SBB_{18}\cap CD_4$ cluster adducts in comparison to that of others. From our simulations, the higher stability of these species compared to $Au_{25}SBB_{18}\cap CD_n$ (where $n < 4$) was attributed to the binding of four CDs in tetrahedral locations (explained later) which would minimize inter-CD interactions and thus lower the total energy of the structure. Second, the tight packing of the four CDs on the cluster surface sterically hinders further CD molecules from interacting with its surface, which also enhances its stability. Data presented in Figure 3 suggest the existence of one dominant supramolecular adduct, $Au_{25}SBB_{18}\cap CD_4$ in solution at a SBB/CD ratio of 1:1.2. Further increase in CD concentration in solution did not result in another species, indicating that addition of more CD molecules onto the cluster surface with retention of the $Au_{25}$ core is unlikely. Ligand-induced core etching was seen at larger concentrations of CD as we have reported previously.[58] The bulky nature of the BBS group may sterically hinder an incoming CD group adjacent to it. Careful control over CD concentration was essential to not cause additional effects. Such control is necessary to achieve specific products in the case of clusters, as seen in the case of ligand exchange and core alloying.[20,54−57] UV−vis absorption spectra (Figure 2B) of these samples showed a nominal decrease in intensity of the characteristic absorption features of the cluster, especially the absorption band found at 685 nm. The ~20 nm shift observed in the UV−vis spectra strongly indicates the modification of the molecule.

$Au_{25}$ QCs are known for their luminescence emission in the near-infrared (NIR) region. In order to study the influence of CD encapsulation on the optical property of $Au_{25}$ QC, we analyzed the NIR luminescence of $Au_{25}$ before and after CD functionalization. The bare $Au_{25}SBB_{18}$ cluster showed a luminescence maximum at 1030 nm at room temperature (see Figure S12). Though various excitation wavelengths showed slight changes in the emission maxima, emission at 1030 nm was the most dominant and intense among others. Upon $\beta$-CD inclusion, the cluster samples showed a pronounced enhancement in their luminescence intensity (Figure 2C). Enhancement of optical properties in such surface-modified clusters is in accordance with previous reports.[59,60] Upon silica coating of $Au_{25}$, both absorption and emission intensities are enhanced.[59] In $Au_{23}SG_{18}$, upon phase transfer, due to additional protection of the cluster by the phase transfer agent, the nonradiative decay rate is reduced, enhancing emission.[60] In the present case, this enhanced luminescence remained almost the same even after 2 weeks in ambient conditions, suggesting the enhanced stability of the cluster as a result of complexation with $\beta$-CD molecules.

Computational studies were conducted in order to ascertain whether the attachment of cyclodextrin molecules to $Au_{25}SBB_{18}$ is feasible and, if so, their locations and the maximum number of such attachments. $Au_{25}$ consists of a 13 atom icosohedral Au core surrounded by six $-S_{nb}-Au-S_b-Au-S_{nb}-$ staples,[37,61] where $S_b$ denote the six bridging sulfurs and $S_{nb}$ the 12 nonbridging sulfurs. The bridging sulfurs join exterior gold atoms to each other in the staple, while the

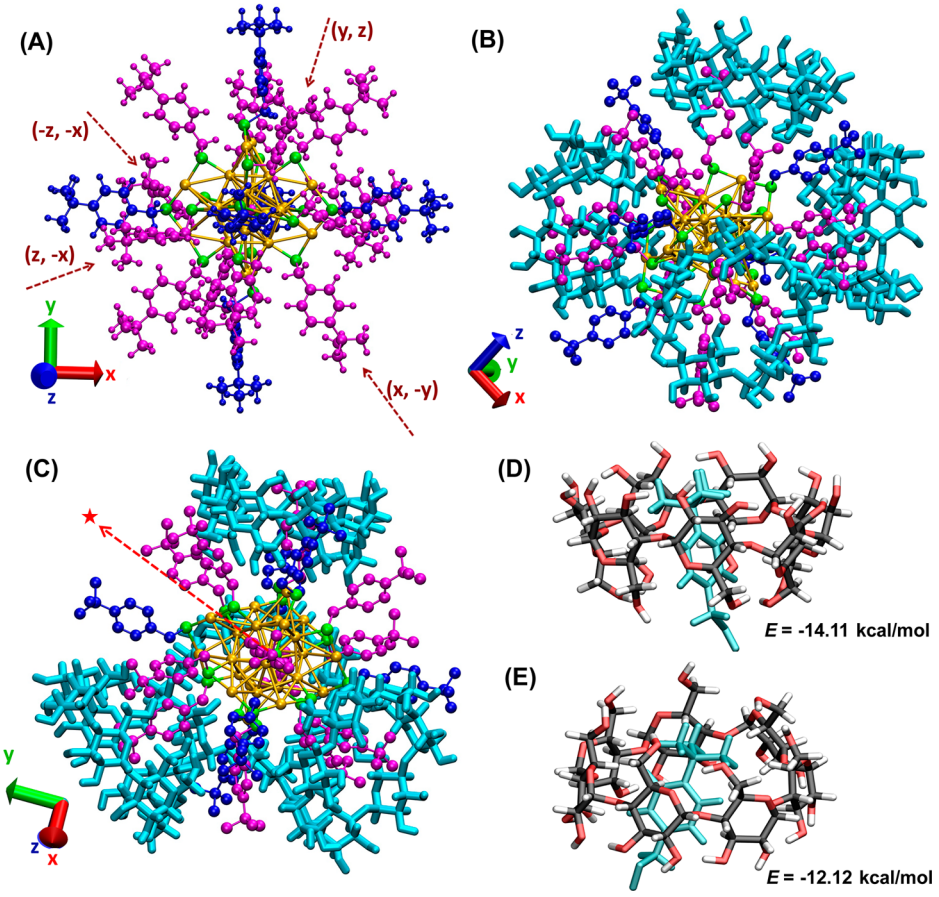


**Figure 4. (A) View of DFT-optimized structure of $Au_{25}SBB_{18}$ where the bridging ligands are shown in blue and the nonbridging ligands in magenta. The ligands identified for the attachment of the four CDs are marked by arrows and by the pairs of Cartesian directions marked next to the arrow. The sulfur and gold atoms are colored green and gold, as in Figure 1A inset, and the Cartesian *x*, *y*, and *z* axes are shown by the red, blue, and green arrows. In the front (B) and back (C) views of $Au_{25}SBB_{18}\cap CD_4$, the hydrogen atoms are not shown on the SBB ligands for clarity. The four CD molecules are shown in cyan in the stick molecular representation and are approximately arranged in a tetrahedral shape. The binding energies in kcal/mol for the isolated BBSH∩CD complexes with the *t*-butyl group of BBSH molecule entering (D) the narrow rim and (E) the wider rim of the CD are shown next to the respective configurations. In (D) and (E), for clarity, all the atoms of the BBSH molecule are shown in one color, cyan, while oxygen, carbon, and hydrogen atoms of CD are shown in red, black, and white, respectively.**

nonbridging sulfurs connect the core Au atoms to an exterior Au atom. Ligands may be classified as bridging (shown in blue color in Figure 4A) and nonbridging (shown in magenta color in Figure 4A), depending on the type of sulfur they are connected to. While the bridging ligands lie 0.5−0.9 Å farther away from the core, as seen in Figure 4A, and are more easily accessible to CDs in solution, they are fewer than the nonbridging ligands. Due to the six two-fold axes of the icosahedral core,[37,61] we rotated the structure so that the SBB bridging ligands lay along the six Cartesian axes *d*, where *d* stands for $\pm x$, $\pm y$, or $\pm z$. The nonbridging ligands may be associated with a Cartesian plane quadrant or diagonal denoted by the pair ($d_1$, $d_2$), where the order of $d_1$ and $d_2$ is unimportant and they are perpendicular. This notation may be used to identify ligands uniquely; the bridging ligands are specified by Cartesian directions, while the nonbridging ligands are specified by a pair of perpendicular directions. If one examines the model of $Au_{25}SBB_{18}$, one can see that the bridging ligands appear to be more crowded, as shown in the inset of Figure 1A and Figure 4A, while there is greater space around the nonbridging ligands. We confirmed this by studying the ligand orientations of the 3D model of $Au_{25}SBB_{18}$ (a structure file is provided in XYZ format along with SI). Hence, it would be possible for a CD to make a closer approach and include a greater portion of a nonbridging rather than a bridging ligand. A closer CD position is in better agreement with the NMR data due to the proximity between the aromatic SBB protons and the $H^3$ and $H^5$ CD protons.

A model of $Au_{25}SBB_{18}\cap CD_4$ is shown in Figure 4B,C, showing the four CDs in an approximately tetrahedral arrangement attached to nonbridging ligands with their narrow end facing the cluster core. A tetrahedral arrangement would be expected to minimize inter-CD interactions. We also note here that the exclusive use of bridging ligands for CD attachment would impose a perpendicular arrangement rather than tetrahedral.

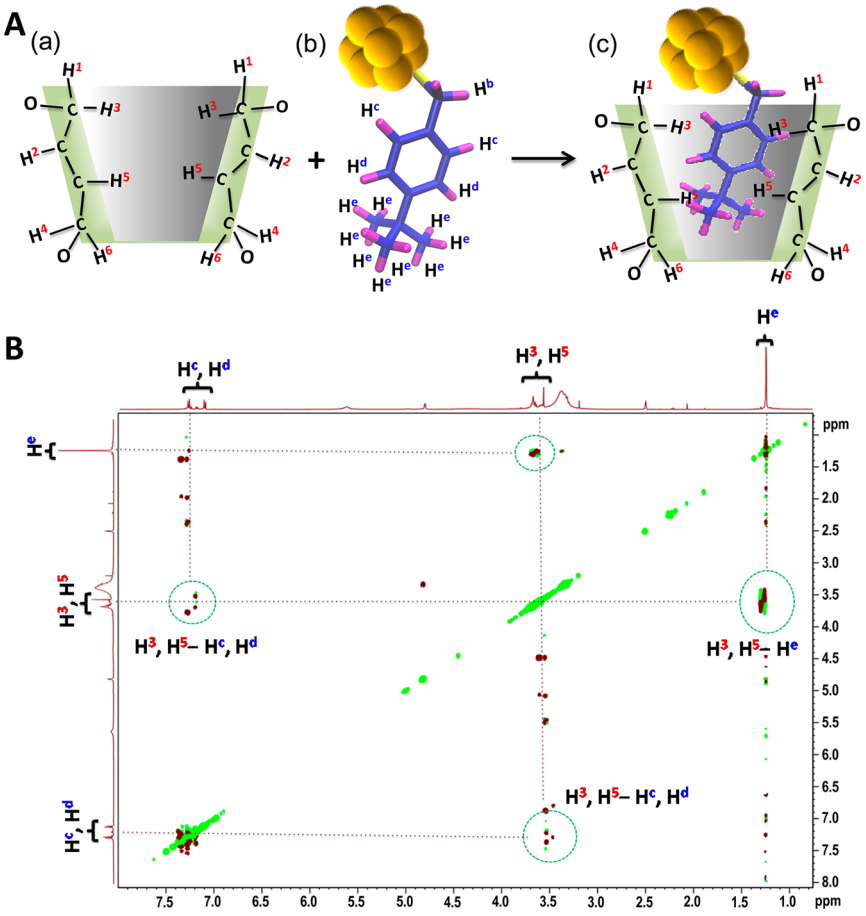


**Figure 5. (A) Schematic showing the inclusion complex between SBB ligand on the QC and $\beta$-CD (a−c represent CD, $Au_{25}SBB_{18}$, and $Au_{25}SBB_{18}\cap CD_4$, respectively). Different types of protons and their interactions are also marked. (B) Two-dimensional ROESY spectrum showing interaction between the inner cavity protons of CD and SBB ligand, which appear as cross-peaks in the spectrum (marked by circles).**

The nonbridging ligands used were denoted by $(-z,-x)$, $(x,-y)$, $(y,z)$, and $(z,-x)$. We remark here that the structure shown in Figure 4B is one possible local minimum and further simulations would be needed to determine the lowest energy structures completely. Structural isomerism is possible as the choice of ligands for CD attachment is non-unique. Full details of the procedure to construct this model may be found in SI 13.

Interestingly, though there are groups of free ligands which are spread over a large space to fit a fifth CD, albeit with tight packing, the specific orientation of free ligands prevents further attachment of another CD. This region of space can be seen in more detail in the back view of the structure shown in Figure 4C (further views are shown in Figure S13). A ligand which appears to have sufficient space around it can be seen at the center of Figure 4C and is marked with a red star. However, it is still too close to the CD at its lower right to enable another CD to be attached to it. This steric hindrance is in striking agreement with the experimental mass spectral results showing four attached CDs as the maximum observed.

Being an efficient tool in CD complexation studies, NMR spectroscopy (especially 2D NMR) can provide information on the details of interaction of $\beta$-CD and the SBB ligands of the cluster such as mode of penetration (through narrow rim or through the wide rim of CD) of the guest molecule, extent of guest inclusion in the CD cavity, orientation of the guest molecule inside the cavity, *etc*. Various protons corresponding to the ligands and that of the CD are marked in the schematic shown in Figure 5. Inner protons in $\beta$-CD are represented as $H^3$ and $H^5$, while the outer protons are marked as $H^1$, $H^2$, $H^4$, and $H^6$. In the case of the SBB ligand, aromatic protons are named as $H^c$ and $H^d$, while *t*-butyl protons and the $CH_2$ protons are represented as $H^e$ and $H^b$, respectively (see Figure 5A). The $^1H$ NMR spectrum of the $\beta$-CD-encapsulated cluster shows induced chemical shifts for certain protons of $\beta$-CD and BBS thiol, which are shown in Figure S14. $\beta$-CD protons were shifted further upfield than parent $\beta$-CD protons, whereas BBS protons were shifted downfield post-encapsulation. The upfield shift of $\beta$-CD cavity protons is attributed to the magnetic anisotropy affects in the $\beta$-CD cavity,[62,63] arising due to the inclusion of

a $\pi$-electron-rich group (here the aromatic ring of BBS). The formation of the supramolecular complex between $\beta$-CD and $Au_{25}SBB_{18}$ cluster was verified by 2D ROESY spectroscopy (Figure 5). This is critical in the study of the interaction between host CDs and guest molecules since protons of both the species are closely located in space after complex formation. The ROESY spectrum of the supramolecular cluster complex shows clear NOE correlations between BBS protons and the protons of $\beta$-CD. Aromatic protons of the BBS group ($H^c$ and $H^d$) show cross-peaks with the inner protons (mainly $H^3$ and $H^5$) of $\beta$-CD. This confirms the formation of an inclusion complex. Moreover, strong cross-peaks were also observed between the protons of the *t*-butyl group ($H^e$) with inner cavity protons of $\beta$-CD, namely, $H^3$ and $H^5$, indicating that they are spatially close to each other. Presence of native as well as complexed *t*-butyl protons was observed in the $^1$H NMR spectra after complexation (pink and green traces in Figure S14), indicating that all the BBS ligands are not complexed with CD. $CH_2$ group protons of BBS ($H^b$) did not show any noticeable cross-peaks with inner $H^3$ and $H^5$ protons of CD in the ROESY spectrum. This may be because the penetration of BBS ligand on $Au_{25}$ into the $\beta$-CD cavity is not deep enough for the group to interact with inner cavity protons of the latter. The 2D COSY experiments also provide information on the coupling of protons between the two moieties. The cross-peaks corresponding to coupling between $H^e$, $H^c$, and $H^d$ protons of the BBS ligand with that of $H^3$ and $H^5$ of CD are marked in Figure S15.

The feasibility of encapsulation of BBSH inside the $\beta$-CD cavity was further confirmed by the detailed analysis of the inclusion complex prepared by the reaction between $\beta$-CD and free BBSH thiol. LDI MS of BBSH∩CD showed the presence of a single sharp peak at *m/z* 1316, which matched well with the theoretical prediction (Figure S16). ESI MS of BBSH∩CD and pure $\beta$-CD are compared in Figure S17. Tandem mass spectrometry data with fragmentation products of peaks at *m/z* 1316 and 1338 corresponding to the loss of BBSH (180 Da) from parent BBSH∩CD are also shown in Figure S17. Binding constant for BBSH∩CD was measured using fluorescence spectral titration (Figure S18). $^1$H NMR and 2D COSY spectrum of BBSH∩CD clearly suggests the complexation between $\beta$-CD and BBSH thiol (Figure S19).

In view of getting more insight into the structure of the most stable inclusion complex, DFT calculations were performed on isolated BBSH∩CD supramolecular adducts. These calculations predict the existence of two different possibilities of encapsulation of BBSH ligand in the $\beta$-CD cavity in solution, that is, either through the wide rim (Figure 4E) or through its narrow rim (Figure 4D). The inclusion complex resulting from the entry of BBSH through the narrow end was more stable by 1.99 kcal/mol than that through the wide rim. However, from the $^1$H NMR data (see Figure S19), we could not precisely determine the chemical shift for the inner and outer protons of CD after complexation since they appeared as broad and diffused peaks. This could be due to the existence of different types of SBB ligands on the cluster surface, namely, the included ones and the unincluded ones on a given cluster (see Figure S14). The former being in two forms (narrow and wider rim entry). Thus, though complexation of CD on $Au_{25}$ was confirmed, the direction of the inclusion was not clearly assignable using NMR data. Such difficulties have been reported previously.[64]

In order to study the specificity of $\beta$-CD in forming a supramolecular complex with BBSH-protected QC, we extended our study to a different QC system of the same core size ($Au_{25}$) but having PET as the protecting ligand (see Experimental Methods section for details). $Au_{25}PET_{18}$ was chosen as it is a well-studied and characterized system.[37,61,65,66] Unlike the SBB ligand which readily forms the inclusion complex, $Au_{25}PET_{18}$ did not show such an effect (black trace in Figure 6) upon treatment with similar concentrations of $\beta$-CD. The spectrum of a $Au_{25}PET_{18}$ + CD mixture shows only a peak due to free $Au_{25}PET_{18}$ at *m/z* 7391. This matches with the theoretical prediction that formation of an inclusion complex on PET-protected $Au_{25}$ may not be facile due to specific orientation of the ligands as noted earlier. This specificity in complexation of the $\beta$-CD cavity for certain ligands was exploited subsequently. A complementary protocol for the incorporation of $\beta$-CD on such clusters would be the replacement of "ligand 1" (PET) with "ligand 2" (BBSH∩CD) on $Au_{25}PET_{18}$. This was achieved by following a simple ligand exchange route. For this, initially the BBSH∩CD complex was prepared (treated as ligand 2) which was subsequently allowed to react with the $Au_{25}PET_{18}$ cluster. This resulted in replacement of three PET ligands by BBSH∩CD (existing as Na adducts, denoted as SBB∩CD-Na as CD-Na interaction is strong) on the QC, which was evident from the MALDI MS data (Figure 6). The well-defined peak in the positive ion mode found at *m/z* 10990 corresponds to the ligand-exchanged product, $Au_{25}PET_{15}(SBB∩CD\text{-}Na)_3$. Loss of the $CH_2{-}CH_2{-}C_6H_5$ group from the ligand, PET, due to C−S cleavage leading to $Au_{25}PET_{14}S_1(SBB∩CD\text{-}Na)_3$ at *m/z* 10884 was also observed. Also, peaks due to the loss of BB∩CD-Na and $CH_2{-}CH_2{-}C_6H_5$ fragments from the cluster leading to $Au_{25}PET_{14}S_2(SBB∩CD\text{-}Na)_2$ and $Au_{25}PET_{13}S_3(SBB∩CD\text{-}Na)_2$ were also identified (marked with red and green stars (*), respectively, in Figure 6). The mass spectrum was in complete agreement with the expected values (see inset of Figure 6). Peaks marked "a" and "b" in the spectrum correspond to the loss of AuL (L = PET) from $Au_{25}PET_{15}(SBB∩CD\text{-}Na)_3$ and $Au_{25}PET_{14}S_2(SBB∩CD\text{-}Na)_2$, respectively. Replacement of PET with a CD-containing ligand did not affect optical absorption spectra of the clusters

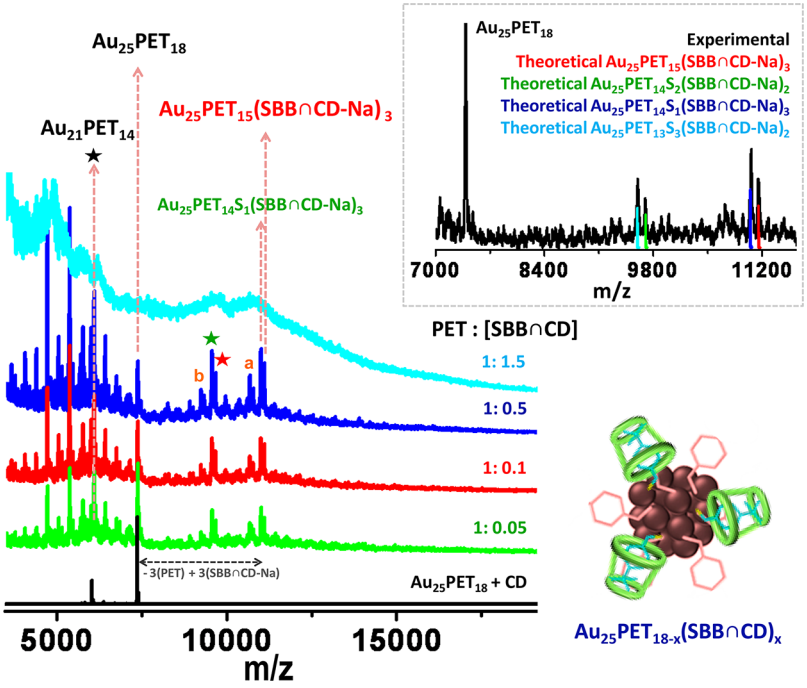


**Figure 6. Positive ion MALDI mass spectra showing the effect of addition of $\beta$-CD (black trace) and increasing amounts of BBSH∩CD (green to cyan trace) to $Au_{25}PET_{18}$. Inset shows the experimental and theoretical match between the predicted values. Ligand-exchanged products are marked in the spectra, and a schematic of the same is also shown. Fragments from the parent cluster are marked with a star.**

significantly (Figure S20) and showed an enhancement of luminescence intensity of the cluster. Note that it is important to exercise careful control over the ratio of PET/SBB∩CD during ligand exchange reactions as evident from the traces, green to cyan in Figure 6. The amount of incoming ligand, SBB∩CD, was deliberately kept low to enable minimal exchange. However, three ligand substitution seems to be the most favored among others.

Surface engineering of QCs by supramolecular chemistry brought many added advantages to the QCs. The instability of QCs, particularly in the presence of certain metal ions, is a major issue in terms of utilizing such materials for commercial applications. Metal-ion-induced quenching of cluster luminescence is a commonly observed phenomenon in most QCs.[36,67−69] While being an efficient metal ion sensor, its application capabilities toward sensing other analytes of interest are limited due to this aspect, especially in complex environments containing multitudes of cations. Interaction with metal ions can also result in irreversible damage to the cluster and also can cause its decomposition.[70,71] Incorporation of CDs on cluster systems has advantages such as increased stability due to lack of accessibility to the core by incoming metal ions and ligands. The stability of $Au_{25}SBB_{18}$∩$CD_4$ over the parent cluster was monitored by their reactivity toward metal ion ($Cu^{2+}$) and other ligands. $Cu^{2+}$ ions react readily with noble metal QCs.[69,72] Here, $Au_{25}SBB_{18}$ and its CD-functionalized analogue, $Au_{25}SBB_{18}$∩$CD_4$, were treated with varying amounts of $Cu^{2+}$ ions (see SI 21 for details), and its effect on cluster luminescence was studied. Though luminescence intensities of both $Au_{25}SBB_{18}$ and its CD-protected analogue were quenched with the addition of $Cu^{2+}$ ions, the extent of quenching observed in $Au_{25}SBB_{18}$∩$CD_4$ was less than that in bare $Au_{25}SBB_{18}$ upon treatment with identical concentrations of $Cu^{2+}$ ions (Figure S21). This may be due to the reduced accessibility of the metal ions to the $Au_{25}$ core owing to the bulky nature of the CD species on the cluster surface. Exposure of the CD-protected cluster ($Au_{25}SBB_{18}$∩$CD_4$) to lower amounts of $Cu^{2+}$ ions (0.05 mL, 250 mM) showed only 30% quenching in its luminescence, whereas $Au_{25}SBB_{18}$ showed 70% quenching. However, with higher amounts of $Cu^{2+}$ ions, the difference in % quenching observed in both cases showed an exponential decrease. This could be due to the effective penetration of the metal ions, owing to their small size, through the protective CD shell around the cluster core. Direct interaction of CD with metal ions, though possible, is unlikely in this case as such interaction requires a highly alkaline medium (pH >12).[73]

The stability of $\beta$-CD-functionalized QCs toward ligand exchange reactions was studied by treating such species with excess ligand of another thiol (thiol-2). This was thought to be another important way to see the difference in core accessibility. $Au_{25}PET_{18}$ was chosen for this study as it gave better mass spectrum compared to $Au_{25}SBB_{18}$ systems, post-complexation. Both bare $Au_{25}PET_{18}$ and $Au_{25}PET_{15}$-(SBB∩CD-Na)$_3$ were treated with excess amounts of thiol-2, in this case free BBSH, and the mass spectrum

was recorded (see Figure S22). In the case of $Au_{25}PET_{18}$, the PET ligands were easily replaced by BBS thiols to give ligand-exchanged products with varying amounts of mixed ligand-protected clusters. But for $Au_{25}PET_{15}(SBB\cap CD\text{-}Na)_3$, the mass spectra showed no shift toward the higher mass region, indicating that ligand exchange was not facile in such systems compared to the bare species. Also, though the CD-functionalized entities were unaffected by BBSH, free $Au_{25}PET_{18}$, which was also present in the solution, showed complete ligand exchange to form $Au_{25}SBB_{18}$ *in situ* (marked on the graph).

Yet another interesting aspect of CDs is their capability in sensing molecules. Competitive guests can replace the existing guests from the CD cavity, and therefore, this can be used in sensing such molecules. An example is provided by 1-adamantanethiol (AdT). Inclusion complexes of CD with adamantyl groups are well-known,[31,74,75] and such products are stable. Many such exchanges of CD guests with adamantyl groups have been reported previously. Both $Au_{25}SBB_{18}$ and $Au_{25}SBB_{18}\cap CD_4$ were treated with the same amount of AdT (Figure S23). Quenching of luminescence was observed in both cases, but in $Au_{25}SBB_{18}$, although an initial decrease in luminescence intensity was noted, probably due to dilution effect/slight ligand exchange, further exposure to AdT did not seem to have an effect on the cluster luminescence. Addition of similar amounts of AdT on $Au_{25}SBB_{18}\cap CD_4$ resulted in substantial reduction of its luminescence intensity (red data points in Figure S23). This effect may be attributed to the fact that, as AdT is a better "guest" for CD than BBS, effective removal of CD from the BBS ligand on the $Au_{25}$ leads to the drastic quenching of luminescence (note that formation of $Au_{25}SBB_{18}\cap CD_4$ resulted in enhanced luminescence). UV optical absorption spectra collected from the samples also gave supporting evidence. While no drastic change was observed upon addition of AdT to bare $Au_{25}SBB_{18}$ clusters, AdT addition to $Au_{25}SBB_{18}\cap CD_4$ indicated gradual evolution of spectral features corresponding to the formation of free $Au_{25}SBB_{18}$ in the solution (green trace in Figure S23D). This reappearance of the $Au_{25}$ cluster features in UV spectra could be due to complex formation between the competitive guest AdT and CD, AdT∩CD, thereby the BBS ligand becomes free on $Au_{25}$ QCs.

## CONCLUSION

In summary, we demonstrated surface functionalization of the $Au_{25}$ clusters based on specific host–guest interactions between $\beta$-CD and (*t*-butyl)benzyl groups of $Au_{25}SBB_{18}$, which imparts new properties to the clusters. A detailed spectroscopic evaluation of the interactions between the QC and $\beta$-CD was conducted. More detailed understanding of the formation of an inclusion complex on the QC surface and a possible structure of $Au_{25}SBB_{18}\cap CD_4$ were provided by DFT calculations and molecular modeling. The observed experimental results were in accordance with the theoretical predictions. The viability of this method in modifying the surface characteristics of differently functionalized QCs has also been demonstrated. Unusual stability and optical properties of CD-functionalized QCs over bare clusters were observed. Our study opens up new possibilities of supramolecular surface-engineered QCs which could overcome some of the limitations of native QCs for potential applications.

## EXPERIMENTAL METHODS

**Materials.** Tetrachloroauric(III) acid ($HAuCl_4\cdot 3H_2O$) and methanol were purchased from SRL Chemical Co. Ltd., India. 4-(*t*-Butyl)benzyl mercaptan ($(CH_3)_3C-C_6H_4-CH_2SH$) (BBSH), 2-phenylethanethiol $C_6H_5-CH_2-CH_2SH$ (PET), 1-adamantanethiol (AdT), and sodium borohydride ($NaBH_4$) were purchased from Sigma Aldrich. $\beta$-CD was purchased from Wako Chemicals, Japan. Tetrahydrofuran was purchased from Rankem, India. All chemicals were of analytical grade and were used without further purification. Glassware was cleaned thoroughly with aqua regia ($HCl/HNO_3$, 3:1 vol %), rinsed with distilled water, and dried in an oven prior to use. Triply distilled water was used throughout the experiments.

**Synthesis of $Au_{25}SBB_{18}$.** $Au_{25}SBB_{18}$ was synthesized using a modified procedure of Jin *et al.* used to prepared $Au_{25}PET_{18}$.[76] In a typical synthesis, 10 mL of $HAuCl_4\cdot 3H_2O$ (14.5 mM in THF) was added to 15 mL of BBSH thiol (89.2 mM in THF) while stirring it at 400 rpm at room temperature (29 °C) in a round-bottom flask. The solution becomes colorless after 15 min, indicating the formation of the Au(I) thiolates. An aqueous solution of 2.5 mL of $NaBH_4$ (0.4 M) was added rapidly to the reaction mixture under vigorous stirring (1100 rpm), and the solution turned from colorless to black, indicating the formation of clusters. The reaction was allowed to proceed with constant stirring for 3 h under ambient conditions and then for 3 h at 45 °C. The crude solution thus obtained had a dark brownish color and showed characteristic UV absorption features of $Au_{25}$ clusters even without any purification. The solution was left overnight to yield monodisperse species. Solvent was removed under vacuum, and the cluster was first washed with water and later precipitated with methanol. The precipitate ($Au_{25}SBB_{18}$) was collected after washing repeatedly with methanol and was dried. For the $Au_{25}PET_{18}$ cluster, the same protocol was followed with the addition of 15 mL of PET (114 mM in THF) instead of BBSH, maintaining other parameters the same.

**Synthesis and Reactivity of $Au_{25}SBB_{18}\cap$CD Systems.** Approximately 3 mg of purified $Au_{25}SBB_{18}$ was dissolved in 3 mL of THF, and 0.1 mL of $\beta$-CD solution (in water) of appropriate concentration was added, such that specific SBB/$\beta$-CD ratio was maintained in the solution (1:0.5, 1:0.8, 1:1, and 1:1.2 for $Au_{25}SBB_{18}\cap CD_n$, where $n = 1-4$, respectively). The mixture was carefully sonicated for about 10 min at room temperature. The reaction was allowed to proceed under constant stirring (400 rpm) for 30 min at room temperature with intermittent sonication for 1 min at every 10 min intervals. After the reaction, the CD-encapsulated clusters were recovered by the addition of excess water, which resulted in the separation of two layers. The deep brown upper layer (organic) was collected and washed with water to remove unbound CD which dissolves in it. Note that free BBSH in the cluster solution that forms an inclusion complex with CD (denoted as BBSH∩CD) will also be removed in this process as it becomes hydrophilic due to CD encapsulation.

Due to the presence of a greater number of hydrophobic BBS groups (in comparison to the BBSH∩CD moieties), CD-functionalized $Au_{25}$ QCs (denoted as $Au_{25}SBB_{18}$∩CD) remained in the organic layer and were used for further studies. SBB/$\beta$-CD mole ratio of 1:1.2, corresponding to $Au_{25}SBB_{18}$∩$CD_4$, was used for detailed experiments unless otherwise mentioned. For sensing experiments with AdT, 1 mg/mL of both the naked and CD-functionalized $Au_{25}SBB_{18}$ was treated with 0.025 and 0.2 mL of 30 mM AdT in THF.

**Instrumentation.** Mass spectral studies were carried out using a Voyager DE PRO biospectrometry workstation (Applied Biosystems) matrix-assisted laser desorption ionization (MALDI) time-of-flight (TOF) mass spectrometer both in the linear and reflectron modes (denoted as MALDI (L) and MALDI (R) MS, respectively) as well as using a MALDI TOF TOF (UltrafleXtreme, Bruker Daltonics) mass spectrometer. In the case of MALDI TOF MS, a pulsed nitrogen laser of 337 nm was employed (maximum firing rate, 20 Hz; maximum pulse energy, 300 $\mu$J) for the measurements. The MALDI TOF TOF mass spectrometer utilizes a 1 kHz smartbeam-II laser, FlashDetector system, and a minimum 4 GHz digitizer. Mass spectra were collected in positive and negative ion modes and were averaged for 500−700 shots. DCTB (trans-2-[3-(4-*t*-butylphenyl)-2-methyl-2-propenylidene]malononitrile) was used as the matrix for all MALDI MS measurements. All spectra were measured at threshold laser intensity to keep fragmentation to a minimum unless otherwise mentioned. Concentration of the analyte and the mass spectral conditions (laser intensity and spectrometer tune files) were optimized to get good quality spectra. UV−vis absorption spectra were collected using a Perkin-Elmer Lambda 25 spectrophotometer. The experiments were carried out at room temperature, and the absorption spectra were recorded from 200 to 1100 nm. Luminescence measurements were done on a Jobin Yvon NanoLog instrument. The band pass for excitation and emission was set at 5 nm. Electrospray ionization (ESI) mass spectrometric measurements were done in the negative mode using LTQ XL, with a mass range of *m/z* 150−4000 and using a Synapt G2 HDMS, quadrupole time-of-flight (Q TOF), ion mobility, orthogonal acceleration mass spectrometer with electrospray (ESI) ionization having a mass range up to 32 kDa. The Synapt instrument used for ESI measurements combined exact-mass quadrupole and high-resolution time-of-flight mass spectrometer with Triwave technology, enabling measurements in TOF mode. The purified samples were dispersed in THF and used for both mass spectrometric measurements. The samples were electrosprayed at a flow rate 5 $\mu$L/min and at a capillary temperature of 150 °C. The spectra were averaged for 80−100 scans. Scanning electron microscopic (SEM) and energy-dispersive analysis of X-ray (EDAX) images were obtained using a FEI QUANTA-200 SEM. For the SEM and EDAX measurements, samples were spotted on a carbon substrate and dried in ambient temperature. Transmission electron microscopy (TEM) was conducted using a JEOL 3011, 300 kV instrument with an ultra-high-resolution (UHR) polepiece. The samples were prepared by dropping the dispersion on amorphous carbon films supported on a copper grid and dried in laboratory conditions. $^1$H NMR and 2D rotating frame nuclear Overhauser effect (ROESY) spectra were recorded on a 500 MHz Bruker Avance III spectrometer operating at 500.15 MHz equipped with a 5 mm smart probe. A 1:1 solvent mixture of 99.9% DMSO-$d_6$ (Aldrich) and 99.9% $CDCl_3$ (SRL) was used to prepare samples and sealed immediately from the laboratory atmosphere. $CDCl_3$ solvent signal served as the reference for the field-frequency lock, and tetramethylsilane was used as the internal reference. All experiments were performed at 25 °C. Standard Bruker pulse programs (Topspin 3.0) were employed throughout. The 1D spectra were acquired with 32K data points. The data for phase-sensitive ROESY experiments were acquired with a spectral width of 4464 Hz in both the dimensions. For each spectrum, 4 transients of 2048 complex points were accumulated for 256 $t_1$ increments and a relaxation delay of 1.975 s was used. A continuous-wave (CW) spin-lock mixing time of 200 ms was employed. Prior to Fourier transformation, zero filling to 1K*1K complex points was performed and apodized with a weighted function (QSINE) in both dimensions. All the data were processed on a HP workstation, using Topspin 3.0 software.

**Theoretical Calculations.** Many properties of QCs have been calculated using DFT efficiently by using smaller $CH_3$ ligands.[77−79] However, here the formation of an inclusion complex requires keeping all the SBB ligands intact, and this increases the CPU resources needed for the calculations significantly. For the computational modeling of $Au_{25}SBB_{18}$, we used density functional theory (DFT) as implemented in the real-space code-package GPAW.[80−82] Structure optimization was performed using full ligands as used in the experiments, Perdew−Burke−Ernzerhof (PBE) functional,[83] 0.2 Å grid spacing, and 0.05 eV/Å criterion for the residual forces for optimization. The GPAW setups for Au include scalar relativistic corrections. The structures of $Au_{25}SBB_{18}$ and $Au_{25}SBB_{18}$∩$CD_4$ were built up with the help of Ecce builder[84] and Avogadro[85] software packages, and visualizations were created with visual molecular dynamics (VMD)[86] software. We generated the initial structure for the optimization of $Au_{25}SBB_{18}$ using a model of $Au_{25}PET_{18}$ taken from one of its known crystal structures[61] and then replacing the PET ligands with SBB ligands. A preoptimization of only the ligand positions, keeping the core and staples fixed, was then carried out using a UFF force field[87] as implemented in Avogadro. The model of $Au_{25}SBB_{18}$∩$CD_4$ was constructed by sequentially attaching four $\beta$-CDs to the DFT-optimized structure of $Au_{25}SBB_{18}$ using Avogadro. The ligand and $\beta$-CD positions of $Au_{25}SBB_{18}$∩$CD_4$ were optimized by the UFF force field[87] keeping the Au and S atoms fixed. The calculations on BBSH∩CD were carried out with Gaussian 09[88] using the B3LYP and hybrid meta-GGA functionals in order to describe the noncovalent forces more accurately, and the basis set was selected according to the size of the system. Further details of all the calculations can be found in the Supporting Information 13.

*Conflict of Interest:* The authors declare no competing financial interest.

*Acknowledgment.* We thank the Department of Science and Technology, Government of India (DST), for constantly supporting our research program on nanomaterials. A.M. thanks CSIR for a research fellowship. T.P., G.N., L.L., and H.H. thank the DST and the Academy of Finland for funding through an Indo-Finland initiative. Mr. T. Karthik, Mr. Mohan, and Mr. Venkadesh are thanked for NMR measurements, and Arun Surendran at Rajiv Gandhi Centre for Biotechnology (RGCB) is thanked for help in mass spectrometric measurements.

*Supporting Information Available:* Additional data on characterization of $Au_{25}SBB_{18}$, $Au_{25}SBB_{18}$∩$CD_4$, and BBSH∩CD adducts along with details of theoretical calculations and optimized structures are provided. XYZ files containing structural coordinates of BBSH∩CD (wide and narrow end entry), $Au_{25}SBB_{18}$, and $Au_{25}SBB_{18}$∩$CD_4$ are also given. Data demonstrating the enhanced stability of the $Au_{25}SBB_{18}$∩$CD_4$ supramolecular adduct and its sensing properties are also provided. This material is available free of charge *via* the Internet at http://pubs.acs.org.

## REFERENCES AND NOTES

1. Daniel, M. C.; Astruc, D. Gold Nanoparticles: Assembly, Supramolecular Chemistry, Quantum-Size-Related Properties, and Applications toward Biology, Catalysis, and Nanotechnology. *Chem. Rev.* **2004**, *104*, 293–346.
2. Burda, C.; Chen, X.; Narayanan, R.; El-Sayed, M. A. Chemistry and Properties of Nanocrystals of Different Shapes. *Chem. Rev.* **2005**, *105*, 1025–1102.
3. Templeton, A. C.; Wuelfing, W. P.; Murray, R. W. Monolayer-Protected Cluster Molecules. *Acc. Chem. Res.* **2000**, *33*, 27–36.
4. Hakkinen, H. The Gold−Sulfur Interface at the Nanoscale. *Nat. Chem.* **2012**, *4*, 443–455.
5. Negishi, Y.; Nobusada, K.; Tsukuda, T. Glutathione-Protected Gold Clusters Revisited: Bridging the Gap between Gold(I)−Thiolate Complexes and Thiolate-Protected Gold Nanocrystals. *J. Am. Chem. Soc.* **2005**, *127*, 5261–5270.

6. Ramakrishna, G.; Varnavski, O.; Kim, J.; Lee, D.; Goodson, T. Quantum-Sized Gold Clusters as Efficient Two-Photon Absorbers. *J. Am. Chem. Soc.* **2008**, *130*, 5032–5033.
7. Shibu, E. S.; Habeeb Muhammed, M. A.; Tsukuda, T.; Pradeep, T. Ligand Exchange of $Au_{25}SG_{18}$ Leading to Functionalized Gold Clusters: Spectroscopy, Kinetics, and Luminescence. *J. Phys. Chem. C* **2008**, *112*, 12168–12176.
8. Udayabhaskararao, T.; Pradeep, T. New Protocols for the Synthesis of Stable Ag and Au Nanocluster Molecules. *J. Phys. Chem. Lett.* **2013**, *4*, 1553–1564.
9. Aikens, C. M. Geometric and Electronic Structure of $Au_{25}(SPhX)_{18}^-$ (X = H, F, Cl, Br, $CH_3$, and $OCH_3$). *J. Phys. Chem. Lett.* **2010**, *1*, 2594–2599.
10. Akola, J.; Walter, M.; Whetten, R. L.; Häkkinen, H.; Grönbeck, H. On the Structure of Thiolate-Protected $Au_{25}$. *J. Am. Chem. Soc.* **2008**, *130*, 3756–3757.
11. Parker, J. F.; Fields-Zinna, C. A.; Murray, R. W. The Story of a Monodisperse Gold Nanoparticle: $Au_{25}L_{18}$. *Acc. Chem. Res.* **2010**, *43*, 1289–1296.
12. Jung, J.; Kang, S.; Han, Y. K. Ligand Effects on the Stability of Thiol-Stabilized Gold Nanoclusters: $Au_{25}(SR)_{18}^-$, $Au_{38}(SR)_{24}$, and $Au_{102}(SR)_{44}$. *Nanoscale* **2012**, *4*, 4206–4210.
13. Kurashige, W.; Yamaguchi, M.; Nobusada, K.; Negishi, Y. Ligand Effects on the Stability of Thiol-Stabilized Gold Nanoclusters: $Au_{25}(SR)_{18}^-$, $Au_{38}(SR)_{24}$, and $Au_{102}(SR)_{44}$ *J. Phys. Chem. Lett.* **2012**, *3*, 2649–2652.
14. Wang, G.; Guo, R.; Kalyuzhny, G.; Choi, J.-P.; Murray, R. W. NIR Luminescence Intensities Increase Linearly with Proportion of Polar Thiolate Ligands in Protecting Monolayers of $Au_{38}$ and $Au_{140}$ Quantum Dots. *J. Phys. Chem. B* **2006**, *110*, 20282–20289.
15. Verma, A.; Stellacci, F. Effect of Surface Properties on Nanoparticle–Cell Interactions. *Small* **2010**, *6*, 12–21.
16. Demchenko, A. P.; Habeeb Muhammed, M. A.; Pradeep, T. Luminescent Quantum Clusters of Gold as Bio-Labels. In *Advanced Fluorescence Reporters in Chemistry and Biology II*; Springer: Berlin, 2010; Vol. 9, pp 333–353.
17. Choi, S.; Dickson, R. M.; Yu, J. Developing Luminescent Silver Nanodots for Biological Applications. *Chem. Soc. Rev.* **2012**, *41*, 1867–1891.
18. Zhou, C.; Long, M.; Qin, Y.; Sun, X.; Zheng, J. Luminescent Gold Nanoparticles with Efficient Renal Clearance. *Angew. Chem., Int. Ed.* **2011**, *50*, 3168–3172.
19. Jin, R. Quantum Sized, Thiolate-Protected Gold Nanoclusters. *Nanoscale* **2010**, *2*, 343–362.
20. Niihori, Y.; Matsuzaki, M.; Pradeep, T.; Negishi, Y. Separation of Precise Compositions of Noble Metal Clusters Protected with Mixed Ligands. *J. Am. Chem. Soc.* **2013**, *135*, 4946–4949.
21. Heinecke, C. L.; Ni, T. W.; Malola, S.; Mäkinen, V.; Wong, O. A.; Häkkinen, H.; Ackerson, C. J. Structural and Theoretical Basis for Ligand Exchange on Thiolate Monolayer Protected Gold Nanoclusters. *J. Am. Chem. Soc.* **2012**, *134*, 13316–13322.
22. Woehrle, G. H.; Brown, L. O.; Hutchison, J. E. Thiol-Functionalized, 1.5-nm Gold Nanoparticles through Ligand Exchange Reactions: Scope and Mechanism of Ligand Exchange. *J. Am. Chem. Soc.* **2005**, *127*, 2172–2183.
23. Zhang, S.; Li, Z.; Samarajeewa, S.; Sun, G.; Yang, C.; Wooley, K. L. Orthogonally Dual-Clickable Janus Nanoparticles *via* a Cyclic Templating Strategy. *J. Am. Chem. Soc.* **2011**, *133*, 11046–11049.
24. Schieber, C.; Bestetti, A.; Lim, J. P.; Ryan, A. D.; Nguyen, T.-L.; Eldridge, R.; White, A. R.; Gleeson, P. A.; Donnelly, P. S.; Williams, S. J.; *et al.* Conjugation of Transferrin to Azide-Modified CdSe/ZnS Core–Shell Quantum Dots Using Cyclooctyne Click Chemistry. *Angew. Chem., Int. Ed.* **2012**, *51*, 10523–10527.
25. Yao, H.; Saeki, M.; Kimura, K. Induced Optical Activity in Boronic-Acid-Protected Silver Nanoclusters by Complexation with Chiral Fructose. *J. Phys. Chem. C* **2010**, *114*, 15909–15915.
26. Rekharsky, M. V.; Inoue, Y. Complexation Thermodynamics of Cyclodextrins. *Chem. Rev.* **1998**, *98*, 1875–1918.
27. Ogoshi, T.; Harada, A. Chemical Sensors Based on Cyclodextrin Derivatives. *Sensors* **2008**, *8*, 4961–4982.
28. Liu, Y.; Chen, Y. Cooperative Binding and Multiple Recognition by Bridged Bis($\beta$-cyclodextrin)s with Functional Linkers. *Acc. Chem. Res.* **2006**, *39*, 681–691.
29. Depalo, N.; Comparelli, R.; Huskens, J.; Ludden, M. J. W.; Perl, A.; Agostiano, A.; Striccoli, M.; Curri, M. L. Phase Transfer of CdS Nanocrystals Mediated by Heptamine $\beta$-Cyclodextrin. *Langmuir* **2012**, *28*, 8711–8720.
30. Chalasani, R.; Vasudevan, S. Cyclodextrin-Functionalized $Fe_3O_4$@$TiO_2$: Reusable, Magnetic Nanoparticles for Photocatalytic Degradation of Endocrine-Disrupting Chemicals in Water Supplies. *ACS Nano* **2013**, *7*, 4093–4104.
31. Park, J. H.; Hwang, S.; Kwak, J. Nanosieving of Anions and Cavity-Size-Dependent Association of Cyclodextrins on a 1-Adamantanethiol Self-Assembled Monolayer. *ACS Nano* **2010**, *4*, 3949–3958.
32. Lehn, J. M. *Supramolecular Chemistry: Concepts and Perspectives*; Wiley-VCH: New York, 1995.
33. Kauffmann, E.; Dye, J. L.; Lehn, J. M.; Popov, A. I. A Study of the Inclusive and Exclusive Cesium Cryptates in Nonaqueous Solvents by Cesium-133 NMR. *J. Am. Chem. Soc.* **1980**, *102*, 2274–2278.
34. Negishi, Y.; Arai, R.; Niihori, Y.; Tsukuda, T. Isolation and Structural Characterization of Magic Silver Clusters Protected by 4-(*tert*-Butyl)benzyl Mercaptan. *Chem. Commun.* **2011**, *47*, 5693–5695.
35. Branham, M. R.; Douglas, A. D.; Mills, A. J.; Tracy, J. B.; White, P. S.; Murray, R. W. Arylthiolate-Protected Silver Quantum Dots. *Langmuir* **2006**, *22*, 11376–11383.
36. Habeeb Muhammed, M. A.; Pradeep, T. Reactivity of $Au_{25}$ Clusters with $Au^{3+}$. *Chem. Phys. Lett.* **2007**, *449*, 186–190.
37. Zhu, M.; Aikens, C. M.; Hollander, F. J.; Schatz, G. C.; Jin, R. Correlating the Crystal Structure of a Thiol-Protected $Au_{25}$ Cluster and Optical Properties. *J. Am. Chem. Soc.* **2008**, *130*, 5883–5885.
38. Angel, L. A.; Majors, L. T.; Dharmaratne, A. C.; Dass, A. Ion Mobility Mass Spectrometry of $Au_{25}(SCH_2CH_2Ph)_{18}$ Nanoclusters. *ACS Nano* **2010**, *4*, 4691–4700.
39. Hapiot, F.; Tilloy, S.; Monflier, E. Cyclodextrins as Supramolecular Hosts for Organometallic Complexes. *Chem. Rev.* **2006**, *106*, 767–781.
40. Villalonga, R.; Cao, R.; Fragoso, A. Supramolecular Chemistry of Cyclodextrins in Enzyme Technology. *Chem. Rev.* **2007**, *107*, 3088–3116.
41. May, B. L.; Gerber, J.; Clements, P.; Buntine, M. A.; Brittain, D. R. B.; Lincoln, S. F.; Easton, C. J. Cyclodextrin and Modified Cyclodextrin Complexes of *E*-4-*tert*-Butylphenyl-4′-oxyazobenzene: UV–Visible, $^1$H NMR and *Ab Initio* Studies. *Org. Biomol. Chem.* **2005**, *3*, 1481–1488.
42. Breslow, R.; Halfon, S. Quantitative Effects of Antihydrophobic Agents on Binding Constants and Solubilities in Water. *Proc. Natl. Acad. Sci. U.S.A.* **1992**, *89*, 6916–6918.
43. Antelo, A.; Jover, A.; Galantini, L.; Meijide, F.; Alcalde, M.; Pavel, N.; Tato, J. Formation of Host–Guest and Sandwich Complexes by a $\beta$-Cyclodextrin Derivative. *J. Inclusion Phenom. Macrocyclic Chem.* **2011**, *69*, 245–253.
44. Ruebner, A.; Yang, Z.; Leung, D.; Breslow, R. A Cyclodextrin Dimer with a Photocleavable Linker as a Possible Carrier for the Photosensitizer in Photodynamic Tumor Therapy. *Proc. Natl. Acad. Sci. U.S.A.* **1999**, *96*, 14692–14693.
45. Schmidt, B. V. K. J.; Hetzer, M.; Ritter, H.; Barner-Kowollik, C. Cyclodextrin-Complexed RAFT Agents for the Ambient Temperature Aqueous Living/Controlled Radical Polymerization of Acrylamido Monomers. *Macromolecules* **2011**, *44*, 7220–7232.
46. Chung, J. W.; Kang, T. J.; Kwak, S.-Y. Guest-Free Self-Assembly of $\alpha$-Cyclodextrins Leading to Channel-Type Nanofibrils as Mesoporous Framework. *Langmuir* **2007**, *23*, 12366–12370.
47. Rusa, C. C.; Bullions, T. A.; Fox, J.; Porbeni, F. E.; Wang, X.; Tonelli, A. E. Inclusion Compound Formation with a New Columnar Cyclodextrin Host. *Langmuir* **2002**, *18*, 10016–10023.

48. Karas, M.; Bahr, U.; Gießmann, U. Matrix-Assisted Laser Desorption Ionization Mass Spectrometry. *Mass Spectrom. Rev.* **1991**, *10*, 335–357.
49. Hillenkamp, F.; Karas, M.; Beavis, R. C.; Chait, B. T. Matrix-Assisted Laser Desorption/Ionization Mass Spectrometry of Biopolymers. *Anal. Chem.* **1991**, *63*, 1193A–1203A.
50. Karas, M.; Bahr, U.; Strupat, K.; Hillenkamp, F.; Tsarbopoulos, A.; Pramanik, B. N. Matrix Dependence of Metastable Fragmentation of Glycoproteins in MALDI TOF Mass Spectrometry. *Anal. Chem.* **1995**, *67*, 675–679.
51. Gross, J.; Leisner, A.; Hillenkamp, F.; Hahner, S.; Karas, M.; Schäfer, J.; Lützenkirchen, F.; Nordhoff, E. Investigations of the Metastable Decay of DNA under Ultraviolet Matrix-Assisted Laser Desorption/Ionization Conditions with Post-Source-Decay Analysis and Hydrogen/Deuterium Exchange. *J. Am. Soc. Mass Spectrom.* **1998**, *9*, 866–878.
52. Zenobi, R.; Knochenmuss, R. Ion Formation in MALDI Mass Spectrometry. *Mass Spectrom. Rev.* **1998**, *17*, 337–366.
53. Whittal, R. M.; Li, L. High-Resolution Matrix-Assisted Laser Desorption/Ionization in a Linear Time-of-Flight Mass Spectrometer. *Anal. Chem.* **1995**, *67*, 1950–1954.
54. Dass, A.; Holt, K.; Parker, J. F.; Feldberg, S. W.; Murray, R. W. Mass Spectrometrically Detected Statistical Aspects of Ligand Populations in Mixed Monolayer $Au_{25}L_{18}$ Nanoparticles. *J. Phys. Chem. C* **2008**, *112*, 20276–20283.
55. Knoppe, S.; Dharmaratne, A. C.; Schreiner, E.; Dass, A.; Bürgi, T. Ligand Exchange Reactions on $Au_{38}$ and $Au_{40}$ Clusters: A Combined Circular Dichroism and Mass Spectrometry Study. *J. Am. Chem. Soc.* **2010**, *132*, 16783–16789.
56. Beqa, L.; Deschamps, D.; Perrio, S. P.; Gaumont, A.-C.; Knoppe, S.; Bürgi, T. Ligand Exchange Reaction on $Au_{38}(SR)_{24}$, Separation of $Au_{38}(SR)_{23}(SR')_1$ Regioisomers, and Migration of Thiolates. *J. Phys. Chem. C* **2013**, *117*, 21619–21625.
57. Kurashige, W.; Munakata, K.; Nobusada, K.; Negishi, Y. Synthesis of Stable $Cu_nAu_{25-n}$ Nanoclusters ($n = 1-9$) Using Selenolate Ligands. *Chem. Commun.* **2013**, *49*, 5447–5449.
58. Shibu, E. S.; Pradeep, T. Quantum Clusters in Cavities: Trapped $Au_{15}$ in Cyclodextrins. *Chem. Mater.* **2011**, *23*, 989–999.
59. Habeeb Muhammed, M. A.; Pradeep, T. $Au_{25}@SiO_2$: Quantum Clusters of Gold Embedded in Silica. *Small* **2011**, *7*, 204–208.
60. Habeeb Muhammed, M. A.; Verma, P. K.; Pal, S. K.; Kumar, R. C. A.; Paul, S.; Omkumar, R. V.; Pradeep, T. Bright, NIR-Emitting $Au_{23}$ from $Au_{25}$: Characterization and Applications Including Biolabeling. *Chem.—Eur. J.* **2009**, *15*, 10110–10120.
61. Heaven, M. W.; Dass, A.; White, P. S.; Holt, K. M.; Murray, R. W. Crystal Structure of the Gold Nanoparticle $[N(C_8H_{17})_4][Au_{25}(SCH_2CH_2Ph)_{18}]$. *J. Am. Chem. Soc.* **2008**, *130*, 3754–3755.
62. Chen, M.; Diao, G.; Zhang, E. Study of Inclusion Complex of $\beta$-Cyclodextrin and Nitrobenzene. *Chemosphere* **2006**, *63*, 522–529.
63. Upadhyay, S.; Ali, S. Solution Structure of Loperamide and $\beta$-Cyclodextrin Inclusion Complexes Using NMR Spectroscopy. *J. Chem. Sci.* **2009**, *121*, 521–527.
64. Maffeo, D.; Leondiadis, L.; Mavridis, I. M.; Yannakopoulou, K. Positive Effect of Natural and Negatively Charged Cyclodextrins on the Stabilization of Penicillins towards $\beta$-Lactamase Degradation Due to Inclusion and External Guest−Host Association. An NMR and MS Study. *Org. Biomol. Chem.* **2006**, *4*, 1297–1304.
65. Dharmaratne, A. C.; Krick, T.; Dass, A. Nanocluster Size Evolution Studied by Mass Spectrometry in Room Temperature $Au_{25}(SR)_{18}$ Synthesis. *J. Am. Chem. Soc.* **2009**, *131*, 13604–13605.
66. Qian, H.; Jiang, D.-E.; Li, G.; Gayathri, C.; Das, A.; Gil, R. R.; Jin, R. Monoplatinum Doping of Gold Nanoclusters and Catalytic Application. *J. Am. Chem. Soc.* **2012**, *134*, 16159–16162.
67. Huang, C. C.; Yang, Z.; Lee, K. H.; Chang, H. T. Synthesis of Highly Fluorescent Gold Nanoparticles for Sensing Mercury(II). *Angew. Chem., Int. Ed.* **2007**, *119*, 6948–6952.
68. Mathew, A.; Sajanlal, P. R.; Pradeep, T. Selective Visual Detection of TNT at the Sub-Zeptomole Level. *Angew. Chem., Int. Ed.* **2012**, *51*, 9596–9600.
69. Habeeb Muhammed, M. A.; Verma, P. K.; Pal, S. K.; Retnakumari, A.; Koyakutty, M.; Nair, S.; Pradeep, T. Luminescent Quantum Clusters of Gold in Bulk by Albumin-Induced Core Etching of Nanoparticles: Metal Ion Sensing, Metal-Enhanced Luminescence, and Biolabeling. *Chem.—Eur. J.* **2010**, *16*, 10103–10112.
70. Xie, J.; Zheng, Y.; Ying, J. Y. Highly Selective and Ultrasensitive Detection of $Hg^{2+}$ Based on Fluorescence Quenching of Au Nanoclusters by $Hg^{2+}-Au^{+}$ Interactions. *Chem. Commun.* **2010**, *46*, 961–963.
71. Huang, C. C.; Yang, Z.; Lee, K. H.; Chang, H. T. Synthesis of Highly Fluorescent Gold Nanoparticles for Sensing Mercury(II). *Angew. Chem., Int. Ed.* **2007**, *46*, 6824–6828.
72. Liu, G.; Feng, D.-Q.; Chen, T.; Li, D.; Zheng, W. DNA-Templated Formation of Silver Nanoclusters as a Novel Light-Scattering Sensor for Label-Free Copper Ions Detection. *J. Mater. Chem.* **2012**, *22*, 20885–20888.
73. Norkus, E. Metal Ion Complexes with Native Cyclodextrins. An Overview. *J. Inclusion Phenom. Macrocyclic Chem.* **2009**, *65*, 237–248.
74. Böhm, I.; Isenbügel, K.; Ritter, H.; Branscheid, R.; Kolb, U. Cyclodextrin and Adamantane Host−Guest Interactions of Modified Hyperbranched Poly(ethylene imine) as Mimetics for Biological Membranes. *Angew. Chem., Int. Ed.* **2011**, *50*, 7896–7899.
75. Harries, D.; Rau, D. C.; Parsegian, V. A. Solutes Probe Hydration in Specific Association of Cyclodextrin and Adamantane. *J. Am. Chem. Soc.* **2005**, *127*, 2184–2190.
76. Wu, Z.; Suhan, J.; Jin, R. One-Pot Synthesis of Atomically Monodisperse, Thiol-Functionalized $Au_{25}$ Nanoclusters. *J. Mater. Chem.* **2009**, *19*, 622–626.
77. Walter, M.; Akola, J.; Lopez-Acevedo, O.; Jadzinsky, P. D.; Calero, G.; Ackerson, C. J.; Whetten, R. L.; Gronbeck, H.; Hakkinen, H. A Unified View of Ligand-Protected Gold Clusters as Superatom Complexes. *Proc. Natl. Acad. Sci. U. S.A.* **2008**, *105*, 9157–9162.
78. Akola, J.; Walter, M.; Whetten, R. L.; Hakkinen, H.; Gronbeck, H. On the Structure of Thiolate-Protected $Au_{25}$. *J. Am. Chem. Soc.* **2008**, *130*, 3756–3757.
79. Lopez-Acevedo, O.; Akola, J.; Whetten, R. L.; Gronbeck, H.; Hakkinen, H. Structure and Bonding in the Ubiquitous Icosahedral Metallic Gold Cluster $Au_{144}(SR)_{60}$. *J. Phys. Chem. C* **2009**, *113*, 5035–5038.
80. Mortensen, J. J.; Hansen, L. B.; Jacobsen, K. W. Real-Space Grid Implementation of the Projector Augmented Wave Method. *Phys. Rev. B* **2005**, *71*, 035109.
81. Enkovaara, J.; Rostgaard, C.; Mortensen, J. J.; Chen, J.; Dułak, M.; Ferrighi, L.; Gavnholt, J.; Glinsvad, C.; Haikola, V.; Hansen, H. A.; *et al.* Electronic Structure Calculations with GPAW: A Real-Space Implementation of the Projector Augmented-Wave Method. *J. Phys.: Condens. Matter* **2010**, *22*, 253202.
82. Bahn, S. R.; Jacobsen, K. W. An Object-Oriented Scripting Interface to a Legacy Electronic Structure Code. *Comput. Sci. Eng.* **2002**, *4*, 56–66.
83. Perdew, J. P.; Burke, K.; Ernzerhof, M. Generalized Gradient Approximation Made Simple. *Phys. Rev. Lett.* **1996**, *77*, 3865–3868.
84. Black, G. D.; Schuchardt, K. L.; Gracio, D. K.; Palmer, B. In *Computational Science - ICCS 2003, International Conference*, Saint Petersburg, Russian Federation, Melbourne, Australia, Proceedings 2660; Sloot, P. M. A., Abramson, D., Bogdanov, A. V., Dongarra, J., Eds.; Springer-Verlag: Berlin, Germany, 2003; Vol. 81, pp 122−131.
85. Hanwell, M.; Curtis, D.; Lonie, D.; Vandermeersch, T.; Zurek, E.; Hutchison, G. Avogadro: An Advanced Semantic Chemical Editor, Visualization, and Analysis Platform. *J. Cheminf.* **2012**, *4*, 1–17.

86. Humphrey, W.; Dalke, A.; Schulten, K. J. VMD - Visual Molecular Dynamics. *Mol. Graphics* **1996**, *14*, 33–38.
87. Rappe, A. K.; Casewit, C. J.; Colwell, K. S.; Goddard, W. A.; Skiff, W. M. UFF, a Full Periodic Table Force Field for Molecular Mechanics and Molecular Dynamics Simulations. *J. Am. Chem. Soc.* **1992**, *114*, 10024–10035.
88. Frisch, M. J.; Trucks, G. W.; Schlegel, H. B.; Scuseria, G. E.; Robb, M. A.; Cheeseman, J. R.; Scalmani, G.; Barone, V.; Mennucci, B.; Petersson, G.; *et al. Gaussian 09*, revision A.1.; Gaussian, Inc.: Wallingford, CT, 2009.